

Lattice mold technique for the calculation of crystal nucleation rates

Jorge R. Espinosa,^a Pablo Sampedro,^a Chantal Valeriani,^{ab} Carlos Vega^a and Eduardo Sanz^{*a}

Received 30th May 2016, Accepted 30th June 2016

DOI: 10.1039/c6fd00141f

We present a new simulation method for the calculation of crystal nucleation rates by computer simulation. The method is based on the use of molds to induce crystallization in state points where nucleation is a rare event. The mold is a cluster of potential energy wells placed in the lattice positions of the solid. The method has two distinct steps. In the first one the probability per unit volume of forming a sub-critical crystal cluster in the fluid is computed by means of thermodynamic integration. The thermodynamic route consists in gradually switching on an attractive interaction between the wells and the fluid particles. In the second step, the frequency with which such cluster becomes post-critical is computed in Molecular Dynamics simulations with the mold switched on. We validate our method with a continuous version of the hard sphere potential and with the sodium chloride Tosi–Fumi model. In all studied state points we obtain a good agreement with literature data obtained from other rare event simulation techniques. Our method is quite suitable for the study of both crystal nucleation of arbitrarily complex structures and the competition between different polymorphs in the nucleation stage.

1. Introduction

Below the melting temperature a crystalline solid is thermodynamically more stable than the fluid. However, many liquids, such as water, can be substantially supercooled in experiments where the presence of impurities is carefully avoided.^{1,2} Fluids can be supercooled because the initial stage of the transition to the solid phase, called crystal nucleation, is a rare event. Crystal nucleation consists in a fluctuation of local order in the metastable liquid that gives rise to a crystalline nucleus whose size and structure are such that it can keep growing.³ Fluctuations leading to small or poorly structured clusters are not successful in nucleating the crystal phase.⁴

^aDepartamento de Química Física I, Facultad de Ciencias Químicas, Universidad Complutense de Madrid, 28040 Madrid, Spain. E-mail: esa01@ucm.es

^bDepartamento de Física Aplicada I, Facultad de Ciencias Físicas, Universidad Complutense de Madrid, 28040 Madrid, Spain

The nucleation stage determines in many cases the structure of the solid obtained by crystallization, which may or may not be that of the most stable crystal phase. In 1897 Ostwald published his famous “step rule” stating that the nucleating phase is that with closest free energy to the fluid.⁵ This rule was reinterpreted in 1933 by Stranski and Totomanow, who claimed that nucleation follows the path with the lowest free energy barrier.⁶ Be it as it may, it is quite important to control which solid phase is formed given that different polymorphs have different physical and chemical properties (solubility, melting temperature, bioavailability, catalytic activity, *etc.*). Therefore, the commercialization of crystalline solids, such as drugs, requires a precise control on polymorphic selection.

The importance of polymorphic selection has motivated intense research activity aimed to understand crystal nucleation. Experimentally it is rather difficult to have access to molecular insight on such a process. Due to its stochastic character, it is not possible to predict when and where in the sample it will take place. It may not occur for a long time but, when it happens, it develops quickly and involves only a small number of molecules. Nonetheless, important efforts have been devoted to observe nucleation experimentally. For instance, colloidal systems, whose constituents are visible with confocal microscopy, have been used to visualize crystal nucleation and growth.⁷ With high-resolution *in situ* transmission electron microscopy (TEM) it has been recently possible to visualize crystal nuclei with an atomic scale.^{8–11} Although promising,¹² these experiments are still far from providing a detailed molecular description of the whole crystal nucleation process.

Computer simulations are an appealing alternative, given that they are cheap as compared to experiments and that they give information at the single-particle level. Although very important advancements have been made in computational studies of crystallization during the past two decades, the work performed so far is mostly limited to simple systems.^{13–15} Rare event methods, like Umbrella Sampling,^{16–30} Forward Flux Sampling,^{21,22,30–34} Metadynamics,^{35,36} or Path Sampling,^{4,37,38} have been used in combination with an order parameter^{39–41} to simulate crystal nucleation. The order parameter labels a tagged particle as solid or as fluid-like based on its local environment and it is required to monitor the growth of the crystal nucleus. This approach works well for solid structures like fcc,¹⁹ bcc⁴² or diamond-like,⁴³ where the local environment is the same for all particles. However, it is not easy to extend this approach to systems with complex symmetry like those typically encountered in industrial or technological applications. For instance ice-V has a monoclinic unit cell of 28 molecules and not all of them have the same environment. Devising a local-environment-based order parameter to study its nucleation with standard rare-event simulation techniques would be extremely complicated.

Here we propose a new methodology for the study of crystal nucleation that bypasses the local-bond order parameter problem. Our approach, which we call Lattice Mold (LM), is based on the use of molds to induce the formation of the crystal nucleus. We have recently shown that the crystal–fluid interfacial free energy can be computed by inducing the formation of a crystal slab in a fluid at coexistence conditions with the aid of a mold of potential energy wells.^{44–46} We use a similar idea here to compute nucleation rates. We validate our method with two systems previously investigated: a system composed of pseudo-hard spheres⁴⁷ and sodium chloride modelled with the Tosi–Fumi interaction potential.^{48,49}

2. The lattice mold method

The main idea of our method, sketched in Fig. 1, is to use a mold to promote crystallization in a metastable fluid. The formation of a crystal cluster is induced with the aid of a mold formed by potential energy wells (represented by empty circles in Fig. 1). When the mold is turned off (wells drawn with dashed lines) particles do not feel the presence of the mold. When it is turned on (wells drawn with solid lines) there is one particle inside each well and a crystal cluster is formed.

By gradually switching on the mold, the reversible work to form the cluster can be computed. If the interaction between the particles and the wells is square-well like with well depth ε_m and well radius r_w , the free energy difference between the fluid and the fluid with the structure generated by the mold is given by:⁴⁴

$$\Delta G^* = \varepsilon_m N_w - \int_0^{\varepsilon_m} d\varepsilon \langle N_{fw}(\varepsilon) \rangle \quad (1)$$

where N_w is the number of wells and $\langle N_{fw}(\varepsilon) \rangle$ is the average number of filled wells for well depth equal to ε . This integral is computed numerically by calculating the integrand in several points by means of NpT simulations keeping fixed the mold position and orientation.

The asterisk in ΔG^* highlights the fact that both the orientation and the center of mass of the mold are fixed. However, unconstrained clusters are free to rotate and translate. We correct the effect of the constraint on the free energy difference as:

$$\Delta G/(k_B T) = \Delta G^*/(k_B T) - \ln(1/(\rho_f V_w)) - \ln(8\pi^2) \quad (2)$$

where k_B is the Boltzmann constant and the second and the third terms in the right hand side account for the translational and orientational free energies of the unconstrained cluster (ρ_f is the fluid number density and V_w the volume of a well, computed as $4/3\pi r_w^3$).

The probability per unit volume to find a crystal cluster in the fluid such as that generated by the mold is given by:

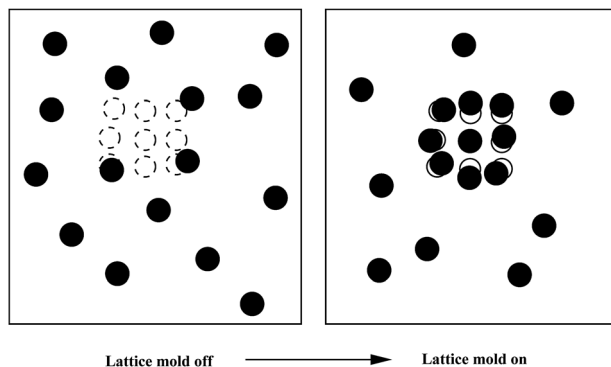


Fig. 1 Schematic representation of how a mold of potential energy wells (empty circles) can induce the formation of a crystal cluster.

$$P = \rho_{\text{f}} e^{-\Delta G/(k_{\text{B}}T)}. \quad (3)$$

In our scheme it is crucial to choose the mold (N_{w} and r_{w}) in such a way that the induced cluster is sub-critical. This implies that when the mold is fully switched on there is an induction period required for the system to crystallize, t . The average induction time, $\langle t \rangle$, can be obtained by averaging t over several independent NpT simulations with the mold fixed and fully switched on. Combining P with $\langle t \rangle$ we obtain the crystal nucleation rate J as:

$$J = P/\langle t \rangle \quad (4)$$

In the “Results” section we give more details on the way the method is implemented in practice by describing the calculation for one particular case.

3. Simulation details

One of the models we use to test our method is the pseudo-hard spheres (PHS) potential, which is a continuous version of the hard sphere potential.⁴⁷ The PHS potential has been shown to closely reproduce the equation of state,⁴⁷ dynamics,⁴⁷ phase diagram,⁵⁰ crystal–fluid interfacial free energy⁴⁴ and crystal nucleation rate^{19,22,51,52} of pure hard spheres. Here we use the same simulation details for PHS as in ref. 44, 50 and 51. To report quantities pertaining to this system we use the particle diameter, σ , as unit of length and as unit of time $\sigma^2/(6D_1)$, where D_1 is the self-diffusion coefficient of the fluid. $\sigma^2/(6D_1)$ is then the “diffusive time”, or the average time a particle takes to diffuse a distance of σ . Pair interactions are truncated at 1.175σ .

We also validate our method with the Tosi–Fumi (T–F) model^{48,49} for NaCl, whose nucleation rate has been previously calculated by Umbrella Sampling²¹ and by seeding.^{46,51} For this model, the melting temperature at 1 bar is 1082 K.⁵³ The simulations details for this system are the same as those given in ref. 46 and 51. We use Particle Mesh Ewald Summations⁵⁴ to deal with electrostatic interactions. The cut-off radius for dispersive interactions and for the real part of electrostatic interactions is 14 Å.

In the Molecular Dynamics simulations carried out in GROMACS⁵⁵ for the NaCl and PHS systems pressure is kept constant using an isotropic Parrinello–Rahman barostat⁵⁶ with a relaxation time of 0.5 ps. To fix the temperature we employ a velocity-rescale thermostat⁵⁷ with a relaxation time of 0.5 ps. The time step for the Verlet integration of the equations of motion is 2 fs in all cases.

To implement the well–particle interaction, v_{wp} , in Molecular Dynamics we use a continuous version of the square-well potential:^{44–46}

$$v_{\text{wp}} = -\frac{1}{2}\epsilon \left[1 - \tanh\left(\frac{r-r_{\text{w}}}{\alpha}\right) \right], \quad (5)$$

where r is the distance between the well and the particle centers, and α is a parameter that controls the steepness of the well’s walls. α cannot be too large to avoid strong forces acting on the particles trapped inside the wells. We use $\alpha = 0.017\text{ Å}$ and $\alpha = 0.005\sigma$ for the NaCl and PHS systems respectively.

The number of particles used to simulate the PHS system was 5324, 2916 and 2048 for $p = 15$, 16 and $17k_{\text{B}}T/\sigma^3$ respectively. For the NaCl system we run simulations with 4096 ions.

4. Results

We use the calculation of the nucleation rate for the PHS model at $p = 16k_{\text{B}}T/\sigma^3$ as a worked example to illustrate our method. For this system we use a mold with 32 wells placed in the lattice positions of a cluster taken from the equilibrium fcc solid at $p = 16k_{\text{B}}T/\sigma^3$ (see Fig. 2). In Fig. 3 we show the integrand of eqn (1) for three different well radii. Each point in Fig. 3 corresponds to an NpT Molecular Dynamics simulation of 33 diffusive times ($\sigma^2/(6D_1)$) in which the mold is kept fixed and interacts with the particles *via* the quasi-square well potential given in eqn (5). Integrating these curves and using eqn (1) and (2) we obtain ΔG for each well radius, as reported in Table 1. We then obtain $\langle t \rangle$ by running typically 10 NpT Molecular Dynamics simulations with the mold switched on with the wells at their maximum depth, ε_{m} . By monitoring the density we can easily identify the time at which each trajectory crystallizes to obtain $\langle t \rangle$ as the average over all trajectories. The trajectories corresponding to $p = 16k_{\text{B}}T/\sigma^3$ and $r_{\text{w}} = 0.35\sigma$ are shown in Fig. 4. In this case we obtain a $\langle t \rangle$ of $3140\sigma^2/(6D_1)$, a much larger time than the $33\sigma^2/(6D_1)$ required to perform thermodynamic integration.

In order for the LM method to work, $\langle t \rangle$ should be as long as one can afford in terms of computational time. In practice this means using molds with the smallest N_{w} and the largest r_{w} for which the system crystallizes in the computational time one can afford. On the one hand, the longer the $\langle t \rangle$ the larger the free energy difference between the state induced by the mold and the top of the barrier separating the fluid from the crystal. Thus, the effect of constraining the crystallization path with a mold is reduced by increasing $\langle t \rangle$. On the other hand, $\langle t \rangle$ must be much larger than the time required to compute a point of the integrand

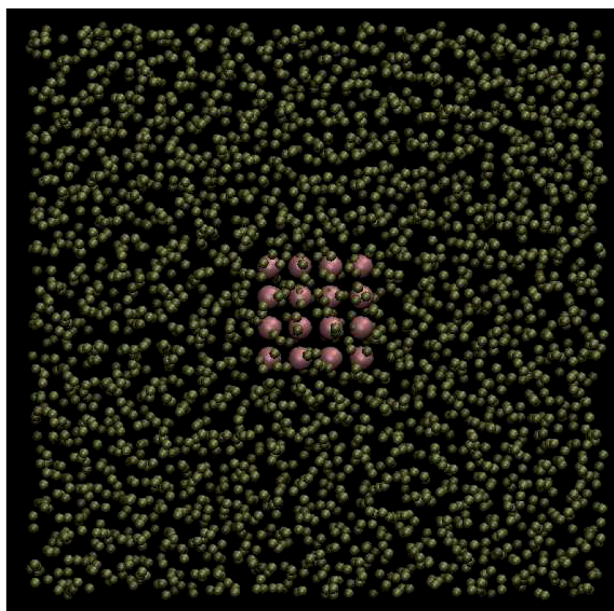


Fig. 2 Big spheres: 32-well lattice mold used for the calculation of J in the PHS system at $p = 16k_{\text{B}}T/\sigma^3$. Small spheres: fluid particles (scaled down to make the mold visible) of the fluid in which the mold is embedded.

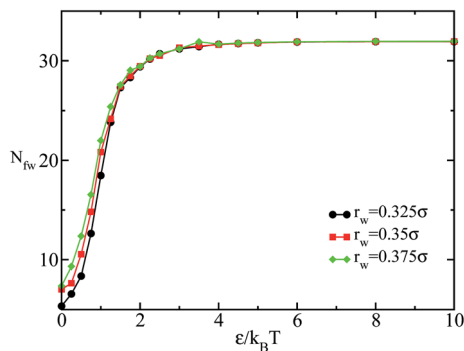


Fig. 3 Number of filled wells (N_{fw}) versus the well depth ($\epsilon/k_B T$) for the PHS model at $\rho = 16k_B T/\sigma^3$ and three different values of the well radius, r_w , as indicated in the legend.

in eqn (1) so that thermodynamic integration can be safely performed without the interference of crystallization. One typically needs tens of diffusive times (1 diffusive time = $\sigma^2/(6D_l)$) to obtain an integrand point. As a rule of thumb we advise the use of molds for which $\langle t \rangle$ is 1 or 2 orders of magnitude larger. By tuning both N_w and r_w we could get molds that satisfy this requirement (Table 1). As one can expect, molds with small N_w and large r_w give large $\langle t \rangle$'s, and *vice versa*.

Once both ΔG and $\langle t \rangle$ have been obtained we compute J using eqn (4). In Fig. 5 we show $\log_{10}(J)$ versus r_w for all pressures studied for the PHS model. The employed molds have the same N_w and different r_w for a given pressure, but different N_w 's are used for different pressures (see Table 1). The larger the pressure the lower the nucleation free energy barrier and the smaller the mold required to induce crystallization. For all studied pressures the logarithm of the nucleation rate increases with r_w and we obtain smaller rates than those predicted in the literature (see Fig. 5 and Table 1). This suggests that we need to extrapolate

Table 1 Nucleation rate, and variables involved in its calculation, for the PHS state points investigated in this work. Pressure p is given in $(k_B T/\sigma^3)$ units and $\langle t \rangle$ in diffusive times, $\sigma^2/(6D_l)$. In the last row of each pressure we report the linear extrapolation of $\log_{10} J$ to r_w^e , which is the definite value of the LM method

p	N_w	r/σ	$\Delta G/(k_B T)$	$\log_{10}[J/(6D_l/\sigma^5)]$	$\rho_l/(\sigma^{-3})$	$\langle t \rangle$
15	83	0.35	43.0	-22.2	1.02	3137
15	83	0.375	39.3	-20.9	1.02	6863
15	83	0.40	36.2	-20.1	1.02	22 745
15		0.485		-16.6		
16	32	0.325	24.0	-13.2	1.01	664
16	32	0.35	22.0	-13.0	1.01	3140
16	32	0.375	19.8	-12.2	1.01	3568
16		0.485		-10.0		
17	14	0.33	10.4	-7.7	0.995	1008
17	14	0.34	10.1	-7.6	0.995	1734
17	14	0.35	10.0	-7.4	0.995	1585
17		0.485		-5.4		

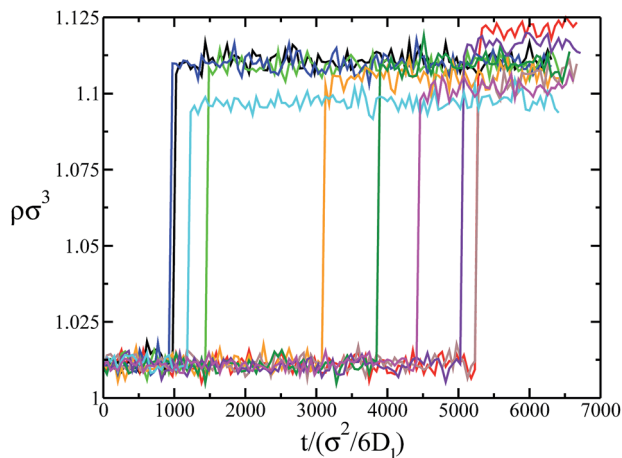


Fig. 4 Density versus time for 10 independent NpT Molecular Dynamics simulations for the PHS system at $p = 16k_B T/\sigma^3$. A 32-well mold with $r_w = 0.35\sigma$ is permanently switched on with $\varepsilon = \varepsilon_m = 10k_B T$.

our results to a larger value of r_w , r_w^e . We try extrapolating to the largest r_w that can be used without having multiple occupancy in the wells. Thus, r_w^e will be given by half the distance at which the inter-particle interaction potential is ε_m ($10k_B T$). This gives $r_w^e = 0.485\sigma$ for the PHS system. For $r_w > r_w^e$ two particles could gain energy by fitting into the same well. Directly calculating the rate at $r_w = r_w^e$ in order to avoid extrapolations would be prohibitively expensive given that $\langle t \rangle$ would be too long. We find that by linearly extrapolating our results to r_w^e we get a good

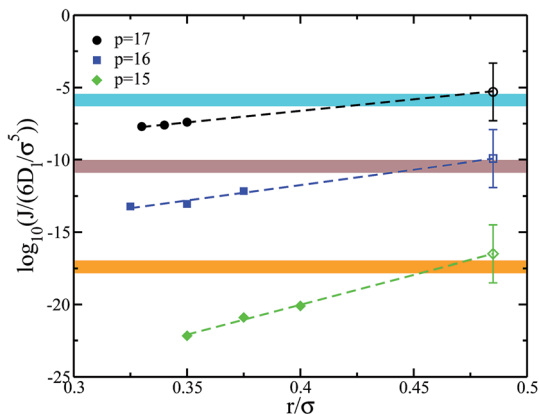


Fig. 5 Solid symbols: nucleation rate computed for different r_w 's for three different pressures of the PHS model as indicated in the legend. Dashed lines: linear fits to $\log_{10} J(r_w)$. Horizontal orange, brown and cyan lines: literature values from US simulations for $p = 15, 16$ and $17k_B T/\sigma^3$ respectively (thickness is comparable to the estimated error bar).^{19,22,52} Empty symbols with error bars correspond to our estimates of the nucleation rate. We give two orders of magnitude error bars. One order comes from the arbitrariness in the determination of r_w^e and another one from the statistical uncertainty of our calculations and the extrapolation to $r_w = r_w^e$.

agreement with previously reported values of J for the three studied pressures (see Fig. 5). The fact that we need to extrapolate our results suggests that for $r_w < r_w^e$ we are artificially restricting those nucleation paths that do not comply with the mold constraint. This does not seem to happen at r_w^e , where we get the right nucleation rate. We acknowledge that the choice of r_w^e is somewhat arbitrary. However, it is worth noting from Fig. 5 that J changes by one order of magnitude (which is a typical error in calculations of the nucleation rate^{21,22}) by changing r_w by 0.03σ . Therefore, we would have given a reasonable value of J by extrapolating to $0.47 < r_w^e < 0.50\sigma$. To compensate for the arbitrariness in the choice of r_w^e we increase by one order of magnitude our error bars in J . As discussed below, we also get good results for the Tosi–Fumi sodium chloride model using this criterion to establish r_w^e .

Following the same procedure we compute the nucleation rate for the Tosi–Fumi sodium chloride model at 800 K and 1 bar. The nucleation rate for such a model at this thermodynamic state was previously computed in ref. 21. In Table 2 we give details of our calculation of J for this system. The runs for the computation of each integrand point in eqn (1) lasted 1 ns. In Fig. 6 we show the nucleation rate as a function of r_w . The value we get for the nucleation rate at r_w^e (1.4 Å) is not in principle in agreement with that reported in ref. 21, which is represented by a horizontal brown line in Fig. 6. There are about 4 orders of magnitude difference between both values, which is beyond the statistical uncertainty. The result of ref. 21 was based on the method developed by Auer and Frenkel¹⁹ that combines a calculation of the nucleation free energy barrier *via* Umbrella Sampling with that of the attachment rate of particles to the cluster, f^+ , to obtain the kinetic prefactor. The free energy barrier reported in ref. 21 has been recently corroborated in the context of a work that combines Hybrid Monte Carlo with Umbrella Sampling to compute nucleation free-energy barriers.⁵⁹ By inspecting the PhD thesis⁵⁸ that led to the publication of ref. 21 we realised that f^+ is $1.3 \times 10^2 \text{ ps}^{-1}$ rather than $1.3 \times 10^{-2} \text{ ps}^{-1}$ as reported in ref. 21 (see Fig. 4.5, Chapter 4, in ref. 58), which accounts for the 4 orders of magnitude difference. The value of ref. 21 corrected by 4 orders of magnitude is shown with a horizontal orange line in Fig. 6. The agreement with our calculation is very satisfactory. Therefore, our method has served to correct the nucleation rate published in ref. 21.

To summarize our results we show in Fig. 7(a) and (b) the nucleation rate *versus* the volume fraction ϕ and the supercooling $\Delta T = T_{\text{melting}} - T$ for the PHS and the Tosi–Fumi NaCl systems respectively. We compare our nucleation rates

Table 2 Nucleation rate, and variables involved in its calculation for the Tosi–Fumi NaCl model at 800 K and 1 bar ($\rho_f = 3.345 \times 10^{28}$ ions per m^3). In the last row we report the linear extrapolation of $\log_{10} J$ to r_w^e , which is the definite value of the LM method. A mold with 18 wells (9 for each ion type) is used for these calculations

N_w	$r_w/\text{Å}$	$\Delta G/(k_B T)$	$\log_{10} J/(\text{m}^{-3} \text{ s}^{-1})$	$\langle t \rangle/\text{ns}$
18	1.1917	15.0	29.9	12.8
18	1.2769	14.4	30.0	16.8
18	1.3620	13.4	30.2	35.4
18	1.4		30.2	

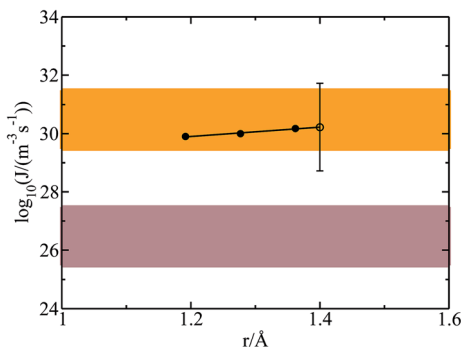


Fig. 6 Solid symbols: nucleation rate computed for different r_w 's for the Tosi–Fumi model of sodium chloride at 1 bar and 800 K. Black solid line: linear fit to $\log_{10} J(r_w)$. Horizontal brown line: literature value (including the error bar) of the nucleation rate.²¹ Horizontal orange line: literature value corrected as discussed in the main text. Empty symbol with error bar corresponds to our estimate of the nucleation rate. We give 1.5 orders of magnitude error bar. 0.75 orders come from the arbitrariness in the determination of r_w^e and the rest from the statistical uncertainty of our calculations and the extrapolation to $r_w = r_w^e$.

with previously published results based on Umbrella Sampling (US),^{19,21,22} Forward Flux Sampling (FFS),^{21,22} Seeding^{46,51} and brute force (BF) calculations.^{22,46} Our results are in excellent agreement with either US or BF calculations in both cases. The seeding technique (red dashed curve) provides a fit based on Classical Nucleation Theory to simulation data obtained by embedding a large crystal cluster in the fluid.^{51,60,61} Despite being an approximate method it captures within 3 orders of magnitude all data from other rigorous techniques. The strength of the seeding method is that it provides an estimate of the nucleation rate over a range of hundreds of orders of magnitude.⁵¹ FFS is in good agreement with US, BF and our method for hard spheres at high densities, but seems to underestimate J for low densities. Also for the NaCl system FFS seems to underestimate J with respect to US, BF and our method.

5. Summary and discussion

In this paper we propose a new method for the calculation of crystal nucleation rates in computer simulations. The method is based on the use of molds to induce crystallization in state points where crystal nucleation is a rare event. The method, which we call Lattice Mold, is divided into two steps. In the first step the probability per unit volume of forming a sub-critical crystal cluster in the metastable fluid is computed by means of thermodynamic integration. The thermodynamic route consists of gradually switching on an attractive interaction between the mold and the fluid particles. In the second step, the frequency with which such a cluster becomes post-critical is computed in Molecular Dynamics simulations with the mold switched on. We validate our method with a continuous version of the hard sphere potential and with the sodium chloride Tosi–Fumi model. In all studied state points we obtain a good agreement with literature data.

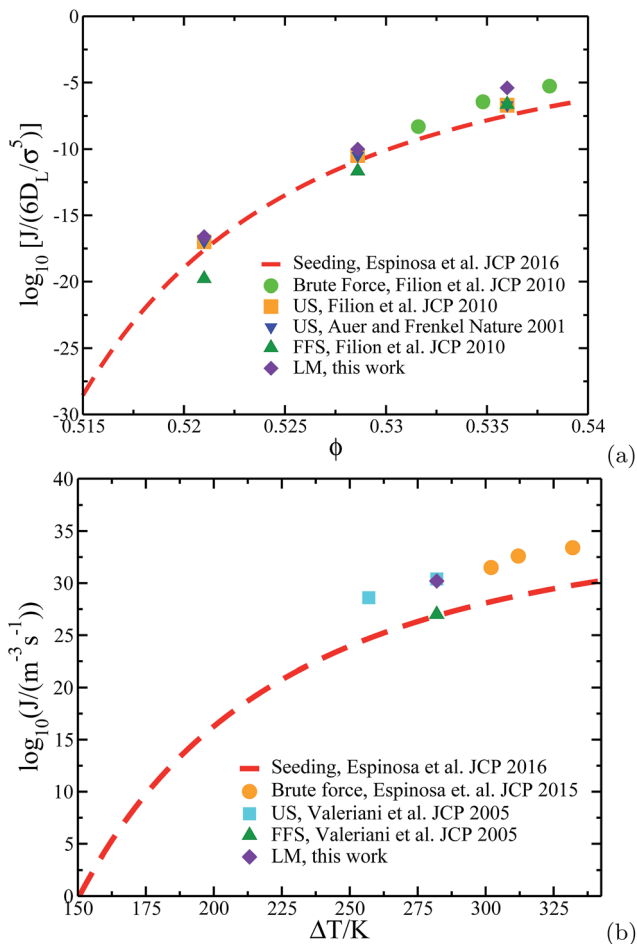


Fig. 7 (a) Nucleation rate for the PHS (this work) and the hard sphere systems (other works as indicated in the legend) as a function of the volume fraction, ϕ . (b) Nucleation rate as a function of the supercooling for the Tosi–Fumi NaCl model at 800 K and 1 bar. The US value from Valeriani *et al.* has been corrected as explained in the main text.

As discussed in the main text, the second step of the calculation is the most computationally demanding since simulations of hundreds/thousands of diffusive times are required. Such simulation times are rather accessible, particularly so because our method can be implemented in efficient Molecular Dynamics simulation packages like Gromacs. As an example, it took us five days to obtain the nucleation rate for a state point of the pseudo-hard sphere model using about 60 CPU nodes. The Lattice Mold is perhaps more demanding than Umbrella Sampling, particularly since it has been shown that the latter can be used in combination with Molecular Dynamics⁵⁹ instead of Monte Carlo. However, we expect Forward Flux Sampling to be more expensive than Lattice Mold, given the huge number of attempts required to estimate the probability to reach the critical cluster.²² The Seeding method is the most efficient way to obtain the nucleation rate in a wide supercooling range,⁵¹ although, unlike Lattice Mold, Umbrella

Sampling or Forward Flux Sampling, it relies on the validity of Classical Nucleation Theory.

In Umbrella Sampling simulations it has been observed that the structure of the cluster core is different from that of the interface in systems like Lennard-Jones or water.^{25,42} This sort of effect could also be captured by the Lattice Mold method given that the induced cluster generates a crystalline halo in such a way that the interfacial structure is not expected to be affected by the presence of the mold in the critical cluster's core. In this respect, it is desirable that the mold is significantly smaller than the critical cluster. For example, the mold used for the calculation of the nucleation rate of pseudo-hard spheres at a reduced pressure of 16 contains 32 wells whereas the critical cluster is expected to have around 120 particles.¹⁹ One knows that the employed mold is sufficiently small if it takes a long time to crystallize the system in the second step of the calculation (hundreds/thousands diffusive times).

In our approach the nucleation pathway is dictated by the mold structure. This issue may be seen as a drawback, but it actually has several advantages over other approaches that rely on the use of local-bond order parameters to detect the growth of crystal clusters. On the one hand, the use of molds enables the study of crystal nucleation through arbitrarily complex structures. It may be quite challenging to find local-bond order parameters for complex solid structures where the local environment changes between different positions of the unit cell. On the other hand, our method enables to rationalise polymorphic selection by comparing the nucleation rate with molds having the structure of all possible polymorphs. For instance, it would be interesting to compare the nucleation rate for fcc and bcc molds in the Lennard-Jones system given that US predicts bcc-like sub-critical nuclei, whereas the stable phase is fcc.¹⁸ Also for the case of water there are different ice polymorphs (ice Ih, ice Ic and ice 0) whose roles in ice nucleation are currently under debate.^{25,62,63} The Lattice Mold method is quite suitable to tackle this sort of problem. Of course, our method would fail in predicting nucleation paths through clusters whose structures are not conceivable *a priori*. In this work we have used molds with the equilibrium structure of the thermodynamically stable solid. The fact that we got a good agreement with other simulation methods suggests that this is a good approximation for the systems here investigated.

Methods like Umbrella Sampling or Forward Flux Sampling are not exempt from making *a priori* assumptions on the nucleation path either. These methods rely on a local-bond order parameter to identify particles belonging to the crystal phase. Such an order parameter is able to discriminate between the fluid and a set of solid structures *a priori* considered as possible candidates for being responsible for crystal nucleation. In Umbrella Sampling or Forward Flux Sampling the structure with the highest nucleation rate among all those consistent with the selected order parameter emerges naturally in the calculations. However, this does not guarantee that a faster nucleation path invisible to the order parameter does not exist.

Our work may inspire experimental groups interested in self-assembly or crystallization. Taking advantage of the fact that nano/micron-sized particles can be trapped by optical tweezers,⁶⁴ small crystalline clusters of colloids have been built up with a lattice mold of optical traps.^{65,66} Optical tweezers could play the role of the potential wells used in this paper to experimentally confine particles and induce crystal nucleation.

Acknowledgements

This work was funded by grants FIS2013/43209-P of the MEC, and by the Marie Curie Career Integration Grant 322326-COSAAC-FP7-PEOPLE-2012-CIG. C. Valeriani and E. Sanz acknowledge financial support from a Ramon y Cajal Fellowship. J. R. Espinosa acknowledges financial support from the FPI grant BES-2014-067625. Calculations were carried out in the supercomputer facility Tirant from the Spanish Supercomputing Network (RES) (project QCM-2015-1-0028).

References

- 1 H. Kanno, R. J. Speedy and C. A. Angell, *Science*, 1975, **189**, 880–881.
- 2 A. Manka, H. Pathak, S. Tanimura, J. Wolk, R. Strey and B. E. Wyslouzil, *Phys. Chem. Chem. Phys.*, 2012, **14**, 4505–4516.
- 3 K. F. Kelton, *Crystal Nucleation in Liquids and Glasses*, Academic, Boston, 1991.
- 4 D. Moroni, P. R. ten Wolde and P. G. Bolhuis, *Phys. Rev. Lett.*, 2005, **94**, 235703.
- 5 W. Ostwald, *Z. Physiol. Chem.*, 1897, **22**, 289.
- 6 I. N. Stranski and D. Totomanow, *Z. Physiol. Chem.*, 1933, **163**, 399.
- 7 U. Gasser, E. R. Weeks, A. Schofield, P. N. Pusey and D. A. Weitz, *Science*, 2001, **292**, 258.
- 8 H. Zheng, R. K. Smith, Y.-w. Jun, C. Kisielowski, U. Dahmen and A. P. Alivisatos, *Science*, 2009, **324**, 1309–1312.
- 9 K. Harano, T. Homma, Y. Niimi, M. Koshino, K. Suenaga, L. Leibler and E. Nakamura, *Nat. Mater.*, 2012, **11**, 877.
- 10 P. J. Smeets, K. R. Cho, R. G. Kempen, N. A. Sommerdijk and J. J. De Yoreo, *Nat. Mater.*, 2015, **14**, 394–399.
- 11 J. M. Yuk, J. Park, P. Ercius, K. Kim, D. J. Hellebusch, M. F. Crommie, J. Y. Lee, A. Zettl and A. P. Alivisatos, *Science*, 2012, **336**, 61–64.
- 12 F. M. Ross, *Science*, 2015, **350**, 1490.
- 13 R. P. Sear, *J. Phys.: Condens. Matter*, 2007, **19**, 033101.
- 14 J. Anwar and D. Zahn, *Angew. Chem., Int. Ed.*, 2011, **50**, 1996–2013.
- 15 G. C. Sosso, J. Chen, S. J. Cox, M. Fitzner, P. Pedevilla, A. Zen and A. Michaelides, *Chem. Rev.*, 2016, **116**, 7078–7116.
- 16 G. Torrie and J. Valleau, *J. Comput. Phys.*, 1977, **23**, 187–199.
- 17 J. S. van Duijneveld and D. Frenkel, *J. Chem. Phys.*, 1992, **96**, 4655.
- 18 P. R. ten Wolde, M. J. Ruiz-Montero and D. Frenkel, *J. Chem. Phys.*, 1996, **104**, 9932.
- 19 S. Auer and D. Frenkel, *Nature*, 2001, **409**, 1020.
- 20 R. Radhakrishnan and B. L. Trout, *J. Am. Chem. Soc.*, 2003, **125**, 7743.
- 21 C. Valeriani, E. Sanz and D. Frenkel, *J. Chem. Phys.*, 2005, **122**, 194501.
- 22 L. Filion, M. Hermes, R. Ni and M. Dijkstra, *J. Chem. Phys.*, 2010, **133**, 244115.
- 23 A. Cuetos and M. Dijkstra, *Phys. Rev. Lett.*, 2007, **98**, 095701.
- 24 A. Reinhardt and J. P. K. Doye, *J. Chem. Phys.*, 2012, **136**, 054501.
- 25 J. Russo, F. Romano and H. Tanaka, *Nat. Mater.*, 2014, **13**, 733.
- 26 I. Saika-Voivod, F. Romano and F. Sciortino, *J. Chem. Phys.*, 2011, **135**, 124506.
- 27 C. Buhariwalla, R. Bowles, I. Saika-Voivod, F. Sciortino and P. Poole, *Eur. Phys. J. E*, 2015, **38**, 39.
- 28 A. V. Brukhno, J. Anwar, R. Davidchack and R. Handel, *J. Phys.: Condens. Matter*, 2008, **20**, 494243.

- 29 P. Geiger and C. Dellago, *J. Chem. Phys.*, 2013, **139**, 164105.
- 30 A. Haji-Akbari, R. S. DeFever, S. Sarupria and P. G. Debenedetti, *Phys. Chem. Chem. Phys.*, 2014, **16**, 25916–25927.
- 31 R. J. Allen, P. B. Warren and P. R. ten Wolde, *Phys. Rev. Lett.*, 2005, **94**, 018104.
- 32 E. Sanz, C. Valeriani, D. Frenkel and M. Dijkstra, *Phys. Rev. Lett.*, 2007, **99**, 055501.
- 33 T. Li, D. Donadio, G. Russo and G. Galli, *Phys. Chem. Chem. Phys.*, 2011, **13**, 19807–19813.
- 34 A. Haji-Akbari and P. G. Debenedetti, *Proc. Natl. Acad. Sci. U. S. A.*, 2015, **112**, 10582–10588.
- 35 A. Laio and M. Parrinello, *Proc. Natl. Acad. Sci. U. S. A.*, 2002, **99**, 12562.
- 36 F. Trudu, D. Donadio and M. Parrinello, *Phys. Rev. Lett.*, 2006, **97**, 105701.
- 37 P. G. Bolhuis, D. Chandler, C. Dellago and P. L. Geissler, *Annu. Rev. Phys. Chem.*, 2002, **53**, 291.
- 38 W. Lechner, C. Dellago and P. G. Bolhuis, *Phys. Rev. Lett.*, 2011, **106**, 085701.
- 39 P. J. Steinhardt, D. R. Nelson and M. Ronchetti, *Phys. Rev. B: Condens. Matter Mater. Phys.*, 1983, **28**, 784–805.
- 40 E. E. Santiso and B. L. Trout, *J. Chem. Phys.*, 2011, **134**, 064109.
- 41 W. Lechner and C. Dellago, *J. Chem. Phys.*, 2008, **129**, 114707.
- 42 P. R. ten Wolde, M. J. Ruiz-Montero and D. Frenkel, *Phys. Rev. Lett.*, 1995, **75**, 2714.
- 43 Z. Zhang, T. Chen and S. C. Glotzer, *Langmuir*, 2006, **21**, 11547.
- 44 J. R. Espinosa, C. Vega and E. Sanz, *J. Chem. Phys.*, 2014, **141**, 134709.
- 45 J. R. Espinosa, C. Vega and E. Sanz, *J. Phys. Chem. C*, 2016, **120**, 8068–8075.
- 46 J. R. Espinosa, C. Vega, C. Valeriani and E. Sanz, *J. Chem. Phys.*, 2015, **142**, 194709.
- 47 J. Jover, A. J. Haslam, A. Galindo, G. Jackson and E. A. Muller, *J. Chem. Phys.*, 2012, **137**, 144505.
- 48 F. Fumi and M. Tosi, *J. Phys. Chem. Solids*, 1964, **25**, 31–43.
- 49 M. Tosi and F. Fumi, *J. Phys. Chem. Solids*, 1964, **25**, 45–52.
- 50 J. R. Espinosa, E. Sanz, C. Valeriani and C. Vega, *J. Chem. Phys.*, 2013, **139**, 144502.
- 51 J. R. Espinosa, C. Vega, C. Valeriani and E. Sanz, *J. Chem. Phys.*, 2016, **144**, 034501.
- 52 S. Auer and D. Frenkel, *J. Phys.: Condens. Matter*, 2004, **120**, 3015.
- 53 J. L. Aragones, E. Sanz, C. Valeriani and C. Vega, *J. Chem. Phys.*, 2012, **137**, 104507.
- 54 D. R. Wheeler and J. Newman, *Chem. Phys. Lett.*, 2002, **366**, 537.
- 55 B. Hess, C. Kutzner, D. van der Spoel and E. Lindahl, *J. Chem. Theory Comput.*, 2008, **4**, 435–447.
- 56 M. Parrinello and A. Rahman, *J. Appl. Phys.*, 1981, **52**, 7182–7190.
- 57 G. Bussi, D. Donadio and M. Parrinello, *J. Chem. Phys.*, 2007, **126**, 014101.
- 58 C. Valeriani, PhD thesis, University of Amsterdam, 2007.
- 59 M. A. Gonzalez, E. Sanz, C. McBride, J. L. F. Abascal, C. Vega and C. Valeriani, *Phys. Chem. Chem. Phys.*, 2014, **16**, 24913–24919.
- 60 B. C. Knott, V. Molinero, M. F. Doherty and B. Peters, *J. Am. Chem. Soc.*, 2012, **134**, 19544–19547.
- 61 E. Sanz, C. Vega, J. R. Espinosa, R. Caballero-Bernal, J. L. F. Abascal and C. Valeriani, *J. Am. Chem. Soc.*, 2013, **135**, 15008–15017.

- 62 B. J. Murray, S. L. Broadley, T. W. Wilson, S. J. Bull, R. H. Wills, H. K. Christenson and E. J. Murray, *Phys. Chem. Chem. Phys.*, 2010, **12**, 10380.
- 63 A. Zaragoza, M. M. Conde, J. R. Espinosa, C. Valeriani, C. Vega and E. Sanz, *J. Chem. Phys.*, 2015, **143**, 134504.
- 64 D. G. Grier, *Nat. Photonics*, 2003, **424**, 810–816.
- 65 M. Hermes, E. C. M. Vermolen, M. E. Leunissen, D. L. J. Vossen, P. D. J. van Oostrum, M. Dijkstra and A. van Blaaderen, *Soft Matter*, 2011, **7**, 4623–4628.
- 66 A. Curran, S. Tuhoy, D. G. A. L. Aarts, M. J. Booth, T. Wilson and R. P. A. Dullens, *Optica* **1**, 2014, 223–226.